

Ultrafast Electron and Energy Transfer in Dye-Sensitized Iron Oxide and Oxyhydroxide Nanoparticles

-- SUPPLEMENTARY TABLE and FIGURES

Table S1. Summary of experimental determinations of the flatband potential, E_{fb} , for hematite and titanium dioxide in aqueous solution at a pH value close to the point of zero surface charge.

References	Sample	pH	E_{fb} (V vs SHE)	Method
Hematite				
Quinn et al., (1976)	Single crystal	8.6	-0.168	Mott-Schottky
Kennedy & Frese (1978)	Polycrystalline electrode	8.9	-0.098	Mott-Schottky
Dimitrijevic et al., (1984)	72-nm diameter colloids	8.6	-0.28	Radiolysis and MV^+/MV^{2+} redox equilibrium
Khan et al., (1999)	Nanocrystal electrode	9*	-0.184	Mott-Schottky
Björkstén et al., 1994)	Nanocrystal electrode	9*	-0.18	Detection of Burstein shift
Titanium dioxide				
Bolts & Wrighton (1976)	Single crystal	6	-0.6	Mott-Schottky
Dimitrijevic et al., (1984)	10-nm diameter colloids	6*	-0.52	Radiolysis and MV^+/MV^{2+} redox equilibrium
Rothenberger et al., (1992)	Nanocrystal electrode	6*	-0.56	Optical absorbance

Footnotes: *For pH values indicated by an asterisk, the measured E_{fb} potential was not performed at the given pH value, but was calculated assuming a Nernstian shift of 0.059 V per pH unit.

References cited in Table S1.

- Björkstén, U., Moser, J. and Gratzel, M. (1994) Photoelectrochemical studies on nanocrystallite hematite films. *Chem. Mater.* **4**, 858-863.
- Bolts, J. M. and Wrighton, M. S. (1976) Correlation of photocurrent-voltage curves with flat-band potential for stable photoelectrodes for the photoelectrolysis of water. *J. Phys. Chem.* **80**, 2641-2645.
- Dimitrijevic, N. M., Savic, D. Micic, O. I. and Novik, A. J. (1984) Interfacial electron-transfer equilibria and flat-band potentials of $\alpha\text{-Fe}_2\text{O}_3$ and TiO_2 colloids studied by pulse radiolysis. *J. Phys. Chem.* **88**, 4278-4283.
- Kennedy, J. H. and Frese, K. W. (1978) Flatband potentials and donor densities of polycrystalline $\alpha\text{-Fe}_2\text{O}_3$ determined from Mott-Schottky plots. *J. Electrochem. Soc.* **125**, 723-726.
- Khan, S. U. M. and Akikusa, J. (1999) Photoelectrochemical splitting of water at nanocrystalline $n\text{-Fe}_2\text{O}_3$ thin-film electrodes. *J. Phys. Chem. B* **103**, 7184-7189.
- Quinn, R. K., Nasby, R. D and Baughman, R. J. (1976) Photoassisted electrolysis of water using single crystal $\alpha\text{-Fe}_2\text{O}_3$ anodes. *Mat. Res. Bull.* **11**, 1011-1018.
- Rothenberger, G., Fitzmaurice, D. and Gratzel, M. (1992) Spectroscopy of conduction band electrons in transparent metal oxide semiconductor films: Optical determination of the flatband potential of colloidal titanium dioxide films.

Nanoparticle Synthesis

All chemicals, used as received, were ACS reagent grade or better. Water was $>18.1\text{ M}\Omega\text{ cm}$ resistivity. Solution pH was adjusted by addition of HCl or NaOH as needed.

Maghemite Nanoparticles. Nanoparticles of magnetite were prepared by co-precipitation of Fe(II) and Fe(III) under anaerobic conditions (37). A freshly prepared solution (3 mL) containing FeCl_2 (0.99 M), $\text{Fe}(\text{NO}_3)_3$ (1.92 M), and NaNO_3 (3.0 M) was slowly added to 40 mL of 6 M NaNO_3 , maintaining a pH of 12 ± 0.1 by the addition of ~6 M NaOH under auto-titrator control (Mettler Toledo T70), resulting in the immediate precipitation of a black solid. This magnetic solid was immediately oxidized in its mother liquor to maghemite by heating to 60 °C and gently bubbling pure $\text{O}_2(\text{g})$ through the suspension for 48 h. Particle suspensions were subsequently centrifuged, decanted, and rinsed with water 3–4 times, and finally re-suspended in a pH 4 solution before use.

Ferrihydrite Nanoparticles. Nanoparticles of ferrihydrite were prepared by precipitation of Fe(III) under anaerobic conditions. A freshly prepared solution (3 mL) containing FeCl_3 (3.1 M) and NaNO_3 (3.0 M) was slowly added to 40 mL of 6 M NaNO_3 , maintaining a pH of 12 ± 0.1 by the addition of ~6 M NaOH under auto-titrator control (Mettler Toledo T70), resulting in the immediate precipitation of a brown solid. Immediately following, the reaction mixture was neutralized to pH ~7 by addition of 1 M HCl, and subsequently dialyzed (in air) against ultrapure H_2O .

Hematite Nanoparticles. Nanoparticles of hematite were prepared by use of a two-step precipitation process (38). First a solution of 200 mL filtered FeCl_3 (2.0 M) with 200 mL of NaOH (5.94 M) was aged in a closed Pyrex bottle at 100 °C for 44 hrs. The sediment was washed with distilled water and freeze-dried, then ball milled with HNO_3 (0.01 M), dispersed by ultrasonic treatment, and centrifuged. The supernatant liquid was used as a seed-solution. To a new solution of 100 mL filtered FeCl_3 (2.0 M) with 100 mL of NaOH (4.8 M) and 100 mL of Na_2SO_4 (0.12 M), 100 mL of the seed solution (~25 mM) was added. The solution was aged at 100 °C for 42 hrs, and the resulting nanoparticle sample was washed in several steps with NH_3 (1.0 M), NaNO_3 (0.5 M), and a 1:1 water/methanol mixture.

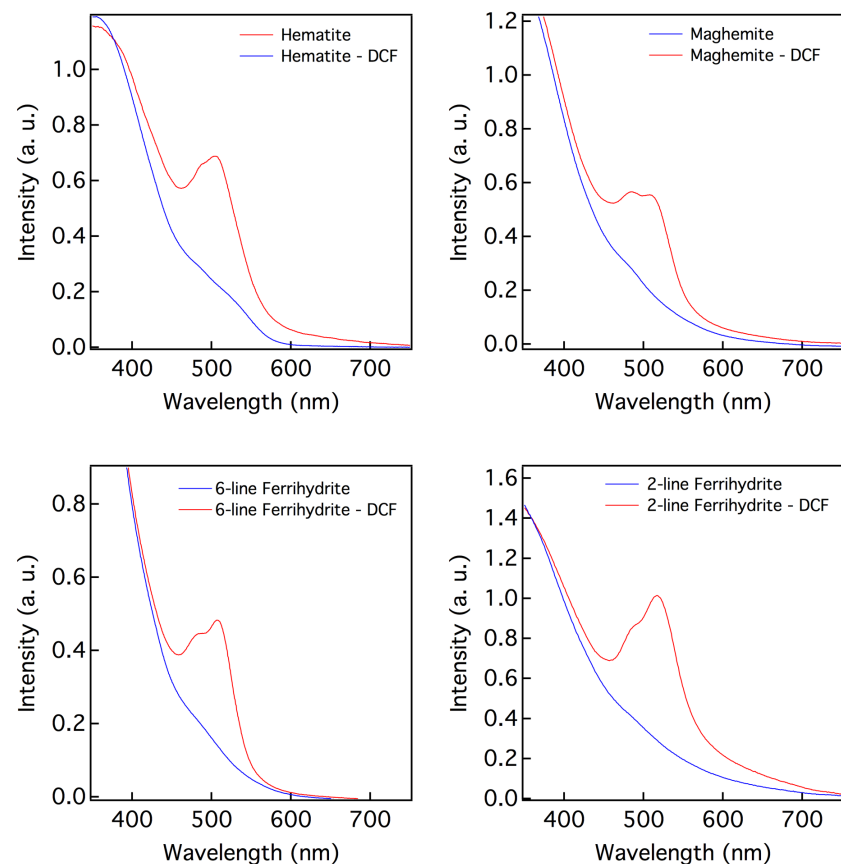


Figure S1. Ground state UV-vis absorption spectra for uncoated and 2',7'-dichlorofluorescein (DCF) nanoparticles.

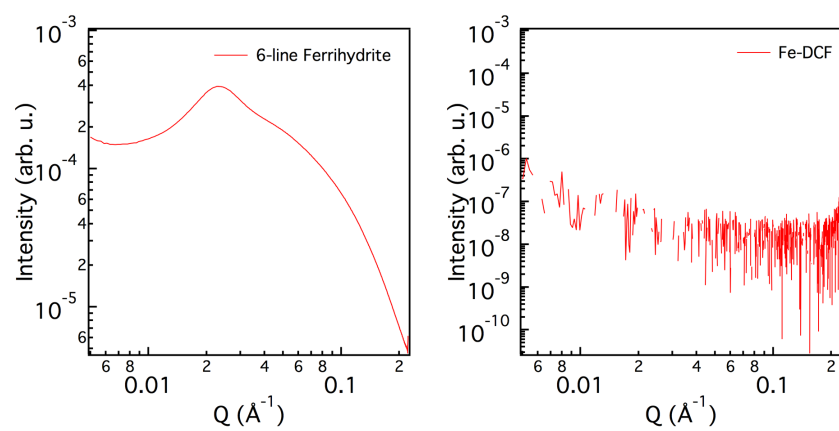


Figure S2. Small-angle X-ray scattering (SAXS) analyses. **A** The background-subtracted SAXS data for suspension of uncoated 6-line ferrihydrite nanoparticles is consistent with a dispersion of charge stabilized nanoparticles with a mean radius of 2.0 nm (Gilbert et al., 2007). **B** The background-subtracted SAXS data for a solution containing ferric iron complexed by 2',7'-dichlorofluorescein (Fe-DCF) reveals only noise, indicating the absence of precipitated particles.

Gilbert, B., G. Lu and C. S. Kim. (2007) *J. Colloid Interf. Sci.* **313** 152-159

Note: All other nanoparticle samples could not be analyzed by SAXS for particle size due to aggregation.

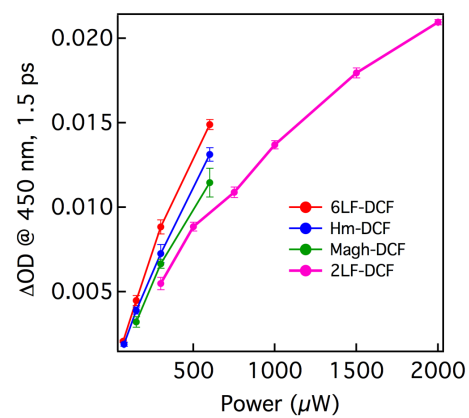


Figure S3. Pump power dependence of the transient absorption signal from 2',7-dichlorofluorescein (DCF) sensitized iron oxide and oxyhydroxide nanoparticles at a probe wavelength of 450 nm and a delay of 1.3 ps. Hm = hematite, M = maghemite, 6LF = six-line ferrihydrite, 2LF = two-line ferrihydrite.

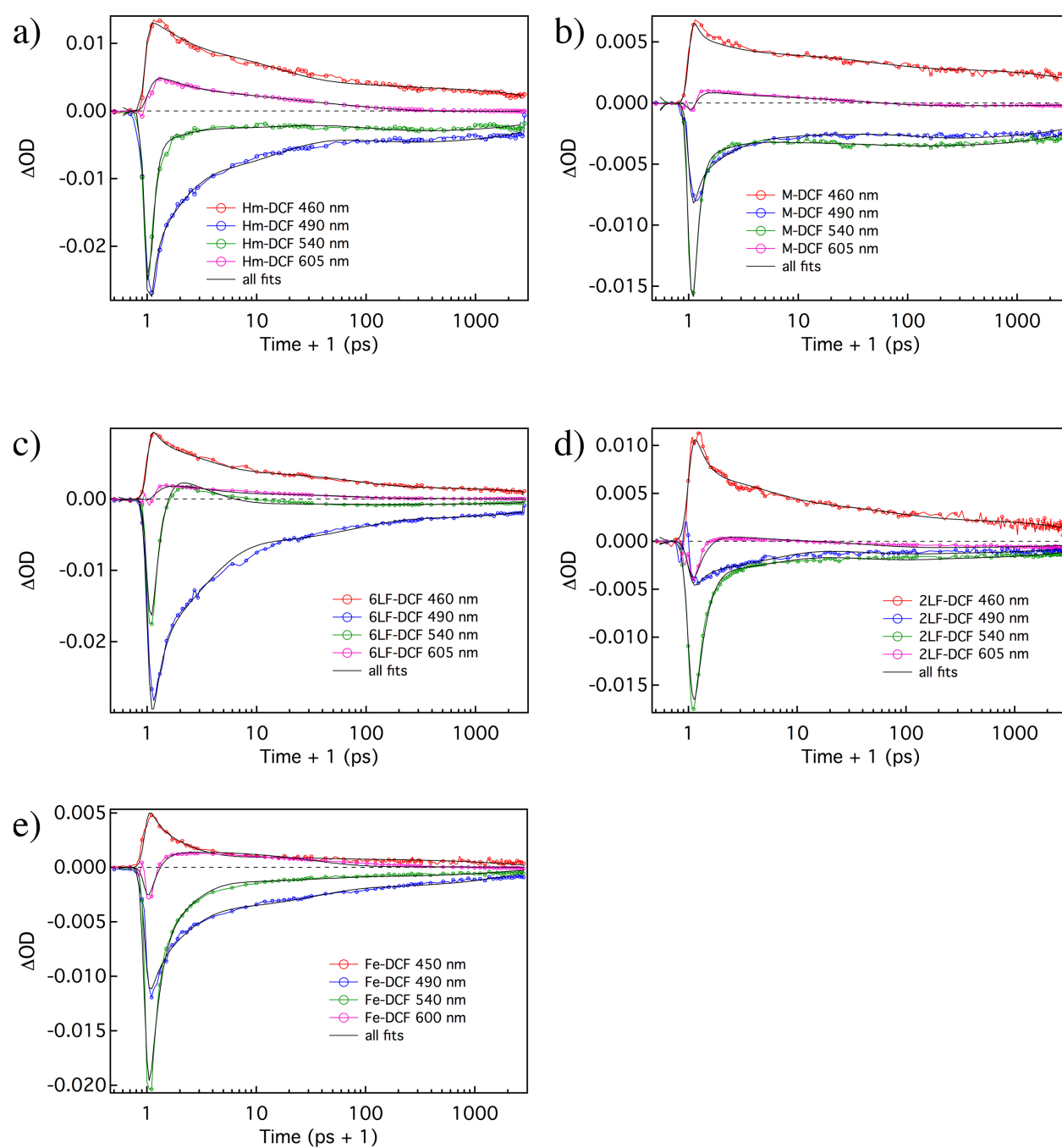


Figure S4. Results of global analyses for all samples. **a)** DCF-coated hematite (Hm). **b)** DCF-coated maghemite (M). **c)** DCF-coated 6-line ferrihydrite (6LF). **d)** DCF-coated 2-line ferrihydrite (2LF). **d)** A cluster compound composed of DCF bound to dissolved iron(III). A 1-ps temporal offset has been added to the time axes for plotting on a logarithmic scale.

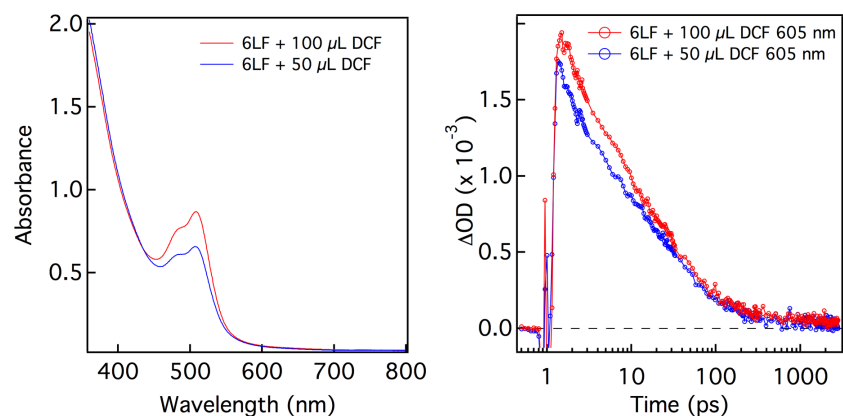


Figure S5. The intensity of the excited state absorption (ESA) observed at 605-nm for DCF-sensitized 6-line ferrihydrite (6LF) is dependent on the amount of dye bound to the nanoparticles. **a)** Ground state UV-vis spectra for two samples of 6LF sensitized with identical iron oxide concentration but with different quantities of dye. **b)** Comparison of the ESA for the two samples shows greater ESA for the higher dye loading.

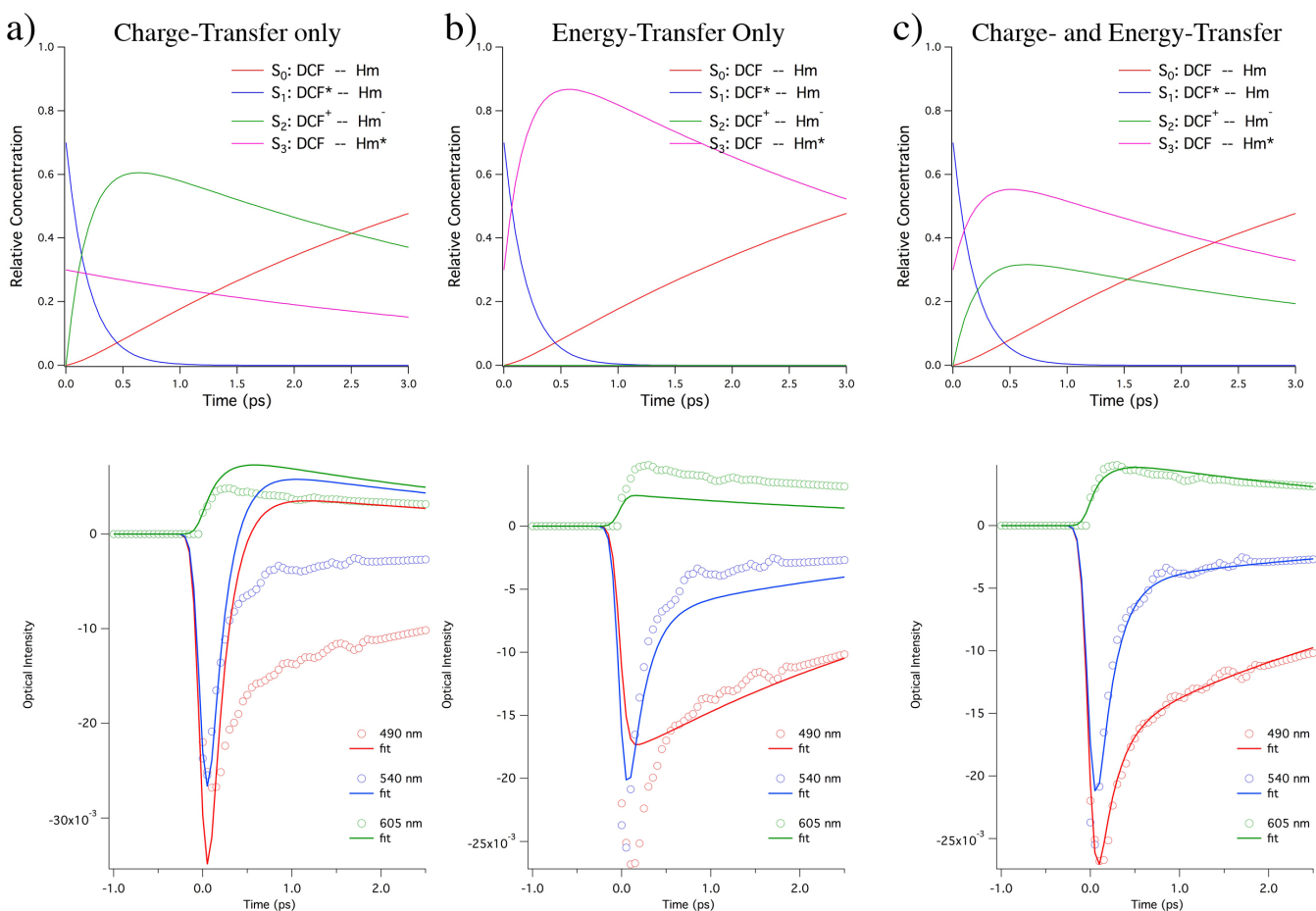


Figure S6. Calculated excited-state population dynamics (top) and associated kinetics (bottom) for three scenarios for dye relaxation pathways. **a)** Charge-transfer only. **b)** Energy-transfer only. **c)** Both charge- and energy-transfer. The charge- and energy transfer rates were chosen so that the lifetime of the dye excited state, S_0 , is the same in all cases. With regard to the transient spectra, the most important distinction between charge- and energy-transfer is that the latter regenerates the dye ground state, leading to the loss of the ground-state bleach signal.

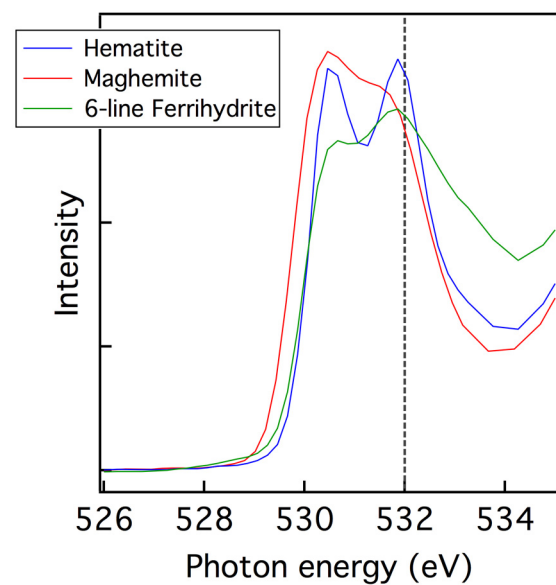


Figure S7. Comparison of the oxygen K-edge X-ray near-edge absorption structure (XANES) spectra for bulk references of hematite and maghemite and one sample of 6-line ferrihydrite nanoparticles. The vertical dashed line is the approximate position of the energy position for electron transfer from the dye excited state.